2021

Numerical Analysis of Active Flow Boiling Regime Management Using a Vapor-Compression Cycle Applied to Electronic Processor Cooling

Riley B. Barta
Purdue University, bartar@purdue.edu

Davide Ziviani

Eckhard A. Groll

Numerical Analysis of Flow Boiling Regime Control Using a Controlled Vapor-Compression Cycle Applied in Electronic Processor Cooling

Riley B. BARTA[1*], Davide ZIVIANI[1], and Eckhard A. GROLL[1]

[1]Ray W. Herrick Laboratories, School of Mechanical Engineering, Purdue University
West Lafayette, Indiana, 47906, USA
riley.barta@tu-dresden.de; dziviani@purdue.edu; groll@purdue.edu

ABSTRACT

As computing power continues to grow at a rapid rate, the thermal load generated from electronic devices follows. Furthermore, reduced size requirements for electronic devices have driven engineers to produce this increased computing power in smaller packaging than ever before. The combination of these two trends results in high heat flux processors that require innovative cooling techniques. Industry and academia alike have anticipated this trend and have developed several general families of solutions to cooling high-heat flux processors. This work proposes the use of flow boiling in a vapor compression cycle and a spreader to distribute the heat from a high-heat flux source to the evaporator. Specifically, the balance between cycle performance and achievable heat flux is assessed, and operating conditions where the ability of the cycle to control evaporator heat flux and simultaneously achieve a high cycle efficiency are identified. A numerical flow boiling correlation is applied and a microchannel evaporator design model is proposed. Geometric parameters and performance limitations of this technique are analyzed and both quantitative and qualitative results along with future work are presented.

1. INTRODUCTION

As traditional forced-air cooling techniques reach their limitations, jet impingement, phase change materials, and flow boiling have become three of the most common strategies to meet these needs, according to Mudawar (2001). To supplement these heat transfer methods, thermoelectric devices have also become common in these applications due to small and modular packaging as well as controllable heat-pumping capacity and surface temperatures, as investigated by Zhang et al. (2010). Gwinn and Webb (2003) found that advances in thermal interface materials such as solder alloys, which are not susceptible to pump out like thermal greases and can be selected to melt at temperatures below the maximum sustainable by either surface, have been shown to reduce thermal resistance between two metal surfaces by an order of magnitude. Joshi and Wei (2005) found that, when implementing two-phase spreading, it has been shown for a given heat flux that the junction temperature can be reduced by up to 37% relative to a solid aluminum plate.

Vapor-compression cycles (VCC) have historically been an effective and reliable means to pump large amounts of heat efficiently. However, these cycles have not seen mainstream application in electronics cooling due to the lack of focus on removing high-heat fluxes and the added complexity and pressures relative to a simple coolant loop operated by a pump. Furthermore, traditional evaporators in vapor-compression cycles are large and are not optimized to absorb high heat fluxes, thus they are generally controlled simply by an expansion valve at the evaporator inlet to ensure superheated vapor exits the heat exchanger before entering the compressor. The significant potential for header maldistrbution due to high flow inlet quality to the evaporator has been a common reason why microchannel evaporators, though more efficient, have not been historically implemented and the fin-and-tube geometry has remained the prevalent for many non-industrial applications. The reduced quality evaporator inlet achieved through the use of a flash tank upstream of the evaporator can help mitigate the maldistribution challenges. With the addition of a phase separator and an evaporator vapor bypass, Tuo and Hrnjak (2012) proved that a microchannel evaporator can be used in an R-134a vapor-compression cycle and can result in increases of 13% - 18% and 4% - 7% for cooling capacity and coefficient of performance (COP), respectively.

While the ability of boiling to cool extreme heat fluxes is not a new concept, controlling the boiling process when subjected to transient conditions has proven the be a source of slow adoption of this technology. In a traditional boiling regime map, the critical heat flux, q''_{CHF}, is a function of several parameters, namely the mass flux, G, pressure, p, the channel diameter, d, and the channel length, L. The target boiling conditions for this work will be to remain in at

approximately 75% of the critical heat flux for a given quality and operating condition in a microchannel heat exchanger. The motivation for this is to balance a high heat flux while not risking dry-out, a common failure mode in cooling applications caused by critical heat flux which results in a rapid rise in surface temperature.

The proposed solution addresses simultaneously a system architecture and control solution, along with a heat exchanger design method, aimed at using flow boiling in a microchannel evaporator to achieve high heat flux cooling. The heat exchanger design method is integrated into the solution scheme to serve the dual purpose of providing the geometric parameters for the heat transfer calculations while also producing a physical design. The proposed design utilizes a vapor-compression cycle with two electronic expansion valves (EXVs), a flash tank phase separator, and a microchannel evaporator mated to a heat spreader mounted on the processor heat source. The microchannel evaporator pressure and outlet superheat serve as inputs to the EXVs and vapor bypass metering valve control scheme. This combination of control and sensory input allows the cycle to vary the evaporator saturation temperature and mass flux through the evaporator, which will maintain the desired flow boiling conditions to remain below critical heat flux during boiling.

2. APPROACH

The target operating condition addressed in this work is to maximize het flux with a maximum source (processor) temperature of 100 °C and a cooling capacity of 525 W from a 50% factor of advancement over the 2020 projection by Sohel et al. (2017). A projection of localized heat flux growth overtime is provided in Figure 1 by Sohel et al. (2017).

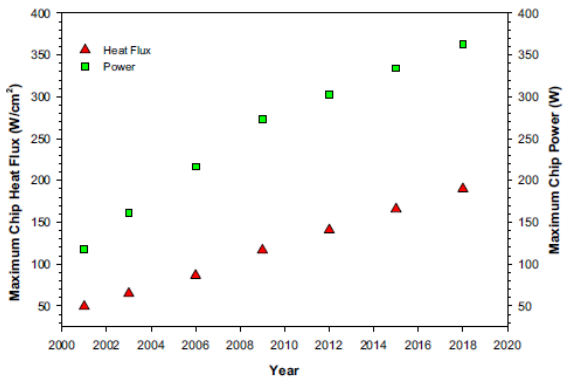

Figure 1: Projection of heat flux growth over time [Sohel et. al (2017)].

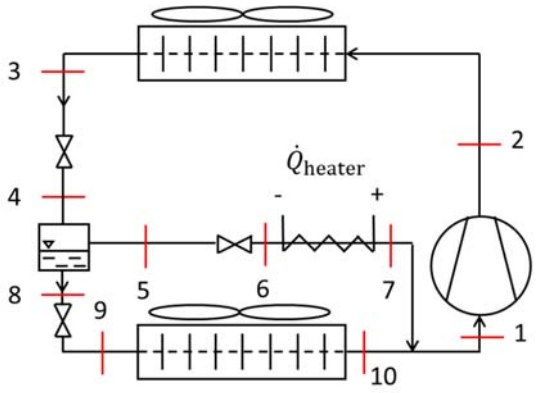

Figure 2: Proposed vapor compression cycle schematic.

This solution will be analytically evaluated in an evenly-distributed heat flux to assess the ability of the technique to dissipate the maximum heat flux produced by the processor over a range of operating conditions. The processor will be soldered to the base of the aluminum microchannel evaporator via solder with low thermal resistance. A schematic of the proposed vapor compression cycle to be used to pump the heat from the chip is shown in Figure 2, with the evaporator located between states 9 and 10.

The proposed solution combines the implementation of enhanced vapor-compression cycle control methods to maintain flow boiling at approximately 75% of the critical heat flux throughout a microchannel evaporator. The analysis conducted herein is focused on using channel boiling in a microchannel evaporator to dissipate heat fluxes on the order of 100 $\frac{\mathrm{W}}{\mathrm{cm}^2}$. Along with these heat fluxes, semiconductor operating temperatures should remain at or below 85 °C - 100 °C and silicon-based power electronics components should remain below 125 °C - 150 °C according to Joshi and Wei (2005).

Given the multi-component nature of this analysis, the analytical approach was split into three distinct efforts:

1. Steady state modeling of a VCC with evaporator flash gas bypass as an additional means of control

2. Modeling of boiling flow regime and variations in saturation temperature of primary working fluid.
3. Design of a microchannel heat exchanger to dissipate the modeled heat flux.

The results of all facets of this analysis will need to be connected to validate a feasible result due to the interconnections of properties between flow regime, channel design, and saturation pressure. In particular, the boiling heat transfer coefficients will need to be calculated through correlations provided in the literature for this specific application. The chosen boiling correlation was developed by Bertsch et al. (2009) for boiling in microchannel evaporators. In addition, this work experimentally validated the correlation with R-134a, which is also the selected refrigerant for this analysis. The correlation calculates the flow boiling heat transfer coefficient, h_{fb}, as a function of the nucleate boiling heat transfer coefficient, h_{NB}, and the convective two-phase heat transfer coefficient, $h_{\mathrm{conv,tp}}$. The nucleate boiling coefficient is the coefficient of a suppression factor that decreases the effect of the heat transfer coefficient with increasing quality to account for dry-out. Furthermore, the calculation of $h_{\mathrm{conv,tp}}$ takes the applied heat flux into account. The convective two-phase coefficient is the coefficient to an enhancement factor term that takes quality and geometric constraining of the flow into account and, among other interrelationships, is ultimately inversely proportional to the flow channel length. Equation 1 shows the form of this calculation.

$$h_{\mathrm{fb}} = h_{\mathrm{NB}}(1-x) + h_{\mathrm{conv,tp}}(1 + a(x^2 - x^6)e^{-bC_{\mathrm{o}}}) \quad [1]$$

The critical heat flux in flow boiling is calculated through a correlation developed by Wu et al. (2010), and is calculated using Equations 2 and 3.

$$Bl_{\mathrm{CHF}} = 0.60\left(\frac{L}{D_{\mathrm{e}}}\right)^{-1.19} x_{\mathrm{e}}^{0.817} \quad [2]$$

$$q"_{\mathrm{CHF}} = Bl_{\mathrm{CHF}} G h_{\mathrm{fg}} \quad [3]$$

Now that the critical heat flux has been found, the applied heat flux can be assessed. For safety, the heat flux applied throughout the cycle is 75% of the critical heat flux. Given the small diameter of the channels utilized, pressure drop was bound to be significant, and thus was calculated for the evaporation portion of the cycle. Equation 4 shows the overall summation of acceleration and friction components of the pressure drop, with Equations 5 and 6 provide detail for the acceleration pressure drop and Equations 7 through 10 provide detail for frictional pressure drop.

$$\Delta P_{2\emptyset} = \Delta P_{\mathrm{accel}} + \Delta P_{\mathrm{friction}} \quad [4]$$

$$\Delta P_{\mathrm{accel}} = G^2 v_{\mathrm{f}}\left[\frac{x_{\mathrm{e,o}}^2}{\alpha_{\mathrm{o}}}\left(\frac{v_{\mathrm{g}}}{v_{\mathrm{f}}}\right) + \frac{(1-x_{\mathrm{e,o}})^2}{1-\alpha_{\mathrm{o}}} - \frac{x_{\mathrm{e,i}}^2}{\alpha_{\mathrm{i}}}\left(\frac{v_{\mathrm{g}}}{v_{\mathrm{f}}}\right) - \frac{(1-x_{\mathrm{e,i}})^2}{1-\alpha_{\mathrm{i}}}\right] \quad [5]$$

where the void fraction, α, is calculated using Equation 6 from Zivi (1964).

$$\alpha = \left[1 + \frac{1-x_{\mathrm{e}}}{x_{\mathrm{e}}}\left(\frac{v_{\mathrm{f}}}{v_{\mathrm{g}}}\right)^{\frac{2}{3}}\right]^{-1} \quad [6]$$

$$\Delta P_{\mathrm{friction}} = \frac{2G^2 L_{2\phi}}{D_{\mathrm{h}} x_{\mathrm{e,o}}} \int_{x_{\mathrm{e,i}}}^{x_{\mathrm{e,o}}} f_{\mathrm{f}} \phi_{\mathrm{f}}^2 (1 - x_{\mathrm{e}}) v_{\mathrm{f}} d_{\mathrm{x,e}} \quad [7]$$

$$X^2 = \left(\frac{\mu_{\mathrm{f}}}{\mu_{\mathrm{g}}}\right)\left(\frac{(1-x_{\mathrm{e}})}{x_{\mathrm{e}}}\right)\left(\frac{v_{\mathrm{f}}}{v_{\mathrm{g}}}\right) \quad [8]$$

$$\phi_{\mathrm{f}}^2 = 1 + \frac{C}{X} + \frac{1}{X^2} \quad [9]$$

where ϕ_f^2 is solved using C from Lee and Garimella (2008) due to its consideration of hydraulic diameter, shown in Equation 10.

$$C = 2566 G^{0.5466} D_{\mathrm{h}}^{0.8819}(1 - e^{-319 D_{\mathrm{h}}}) \quad [10]$$

In order to accurately model the multi-phase nature of heat exchanger within a VCC, a segmented heat exchanger model was selected. This model takes a given step size, being a physical geometry step or a fixed change in specific enthalpy, and depending on the state of the flow for a given section, the properties of the flow for that region are calculated with the appropriate correlations. Once the boundaries of a given segment have been established through iterative comparison of the temperature of the working fluid to the saturation temperature for the operating pressure, the appropriate heat transfer and pressure-drop correlations are applied. A schematic and flow chart to offer visual support of this process are shown in Figure 3 and Figure 4, respectively, with the flowchart focusing on the two-phase region calculations.

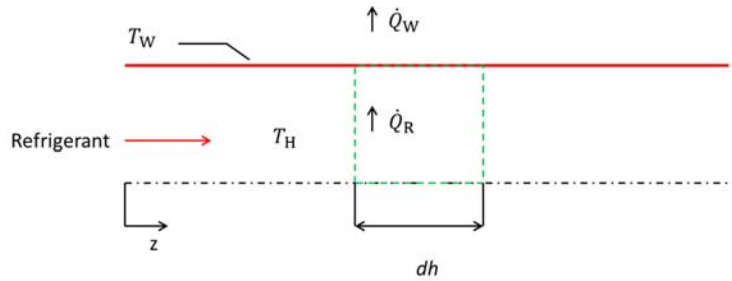

Figure 3: Segmented heat exchanger schematic.

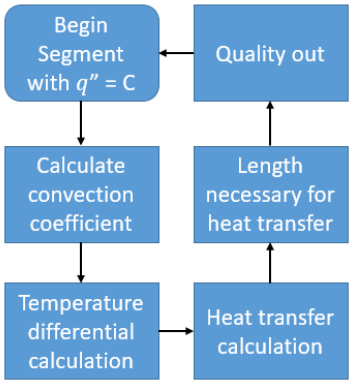

Figure 4: Segmented heat exchanger flowchart.

Referring to the schematic provided in Figure 2, the proposed control scheme for the cycle would be to use the high-pressure EXV between states 3 and 4 to regulate the liquid level in the flash tank and condenser outlet sub-cool. Combined with the low-pressure EXV located between states 8 and 9 and the flash gas bypass valve located between states 5 and 6, the flash tank pressure can be varied. The low-pressure EXV would also control the evaporator outlet superheat, while reaching a balance in pressure differential across the flash gas bypass valve to achieve a steady flash tank liquid level. It should be noted that this control scheme description only describes the primary function of each valve, and that in reality modulation of each valve would have an effect on the ability of both other valves to achieve a given effect on the system. Therefore, an applied control scheme would need to take the flash tank pressure, flash tank liquid level, and evaporator outlet superheat into consideration simultaneously to successfully control the system, at which point the decision as to which valve should be modulated becomes a question of relative impact of each valve on the desired variation in operating condition. In initial investigations, a heater is applied to the vapor bypass line between states 6 and 7 for compressor safety. Theoretically, the compressor suction superheat would be used as a control input parameter such that the evaporator superheat could be controlled via the low-pressure EXV to offset the mixing with the high-quality vapor in the bypass line. However, until a robust control strategy is developed and experimentally-validated, the heater is retained for the sake of system safety and conservative design.

3. SYSTEM OPTIMIZATION

As mentioned in the correlation descriptions, there is a direct connection between the geometry, heat transfer coefficient, and the resulting heat flux. In order to capture this relationship as well as possible, the segmented heat transfer heat exchanger is partitioned in sections of specific enthalpy, not geometric sections as is traditionally done. This was in order to ease the integration of the heat exchanger model in the vapor-compression cycle, but also has the effect of varying geometric length for each partition of specific enthalpy, thus shifting this tool from an analysis tool to a design tool. This segmentation process is shown in Equations 11, 12, and 13.

$$\Delta h_{\text{segment}} = \frac{\dot{Q}}{\dot{m} n_{\text{segments}}} \quad [11]$$

$$\dot{Q}_{\text{segment}} = \dot{m} \Delta h_{\text{segment}} \quad [12]$$

$$\dot{Q}_{\text{segment}} = h_{\text{fb}} A_{\text{segment}} \Delta T \quad [13]$$

where

$$A_{\text{segment}} = \pi D_{\text{h}} L_{\text{segment}} \quad [14]$$

and

$$\Delta T = T_{\text{surface}} - T_{\text{evap}} \quad [15]$$

The total length of the tubing needed to achieve the desired cooling is calculated through Equation 16.

$$L_{\text{tot}} = \sum_{i=1}^{n_{\text{segment}}} L_{\text{i}} \quad [16]$$

While the summation of the local lengths seems straightforward, the ratio of the local segment length to the flow path diameter is directly proportional to the critical heat flux for that given segment as shown in Equation 2. The interrelationships between heat exchanger length and heat transfer rate have been discussed, and it should be noted that the geometric L_{tot} calculated in the first iteration of Equation 16 is likely not exactly the L used in the h_{tp} correlations. These two lengths need to match in order to accurately design the heat exchanger, therefore a solution scheme needed to be developed to solve for the geometry that would both allow for adequate heat rejection and agree with the heat transfer correlation outputs. In other words, the assumed length needs to be a variable that is iterated upon until the length that is used in the heat transfer correlation matches the geometric length used. A flow chart for this solver is provided in Figure 5.

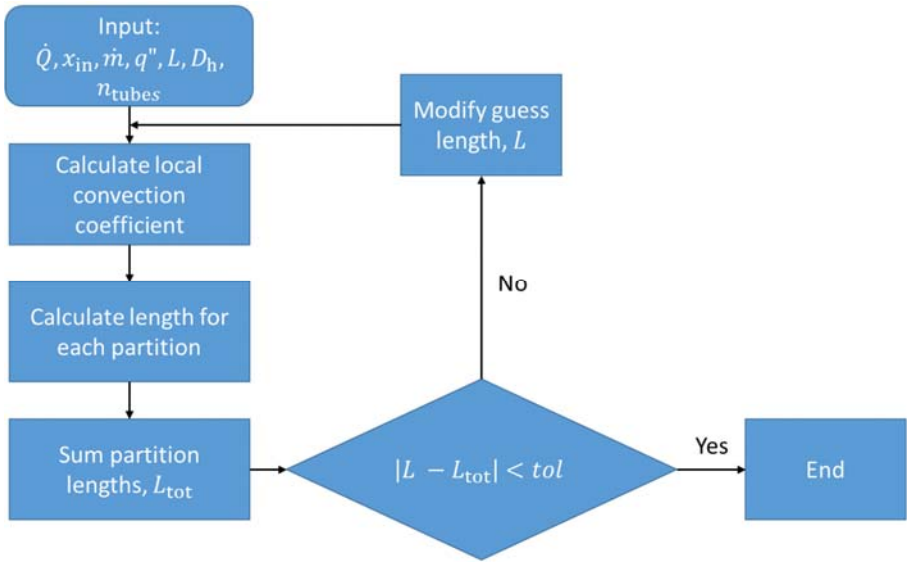

Figure 5: Heat exchanger geometry flowchart.

While this is the calculation for the total length necessary for heat transfer in a single tube, this value can be decreased with a number of parallel tubes in order to decrease the overall length of the heat exchanger. This will then increase the width of the heat exchanger, and this dimension as well as all others used to obtain a true geometry for the surface of the heat exchanger is outlined in Figure 6. The effective heat transfer area, $A_{\text{evap,base}}$, allows the calculation of the heat flux that can be dissipated from the spreader and is calculated as a simple rectangle using the product of length and width.

Finally, the vapor-compression cycle is modeled at an ambient condition of 25 °C with an assumed outlet pinch of the condenser at 5 K and a source, or chip surface, temperature of 90 °C was chosen. The condenser outlet sub-cool is set at 5 K, and the compressor suction superheat is maintained at 10 K with a constant capacity, suggesting a variable-

speed compressor at a constant isentropic efficiency of 70%. A constant heat exchanger pinch point of 5 K is assumed, and the evaporator outlet state is assumed to be saturated vapor in this investigation due to the focus being on two-phase behavior. Therefore, the heater on the vapor bypass line is used to provide the additional heat input to satisfy the compressor suction superheat target. The evaporator pressure is a variable value, given that the temperature differential between the chip surface and the investigated evaporation temperatures is large in order to maximum heat transfer. The flash tank phase separation is assumed to be ideal. A schematic and pressure – specific enthalpy (P-h) diagram of this vapor-compression cycle solution are provided in Figure 2 and Figure 7, respectively.

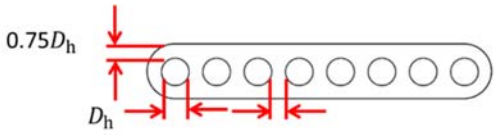

Figure 6: Microchannel heat exchanger dimensions as a function of D_h.

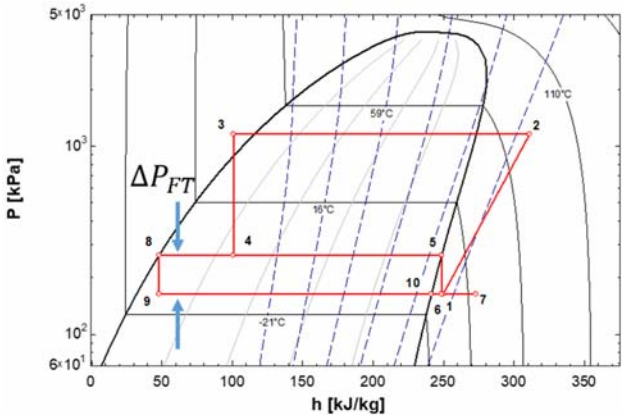

Figure 7: Theoretical P-h diagram of proposed cycle.

The heat spreader provided the surface temperature of the evaporator and was calculated using a simplified thermal resistance network that considers conduction and spreading resistance through the spreader, as shown by Equations 17, 18, 19, and 20. The spreader was assumed to be Aluminum with a thermal conductivity, *k*, of 200 $\frac{\mathrm{W}}{\mathrm{m-K}}$.

$$\dot{Q} = \frac{T_{\mathrm{chip}} - T_{\mathrm{surface}}}{R_{\mathrm{eq}}} \quad [17]$$

$$R_{\mathrm{eq}} = R_{\mathrm{cond}} + R_{\mathrm{sp,max}} \quad [18]$$

$$R_{\mathrm{cond}} = \frac{th_{\mathrm{sp}}}{k_{\mathrm{sp}} A_{\mathrm{sp}}} \quad [19]$$

$$R_{\mathrm{sp,max}} = \left[\frac{\sqrt{A_{\mathrm{evap,base}}} - \sqrt{A_{\mathrm{chip}}}}{k_{\mathrm{sp}}\sqrt{\pi A_{\mathrm{evap,base}} A_{\mathrm{chip}}}}\right] \cdot \left[\frac{\frac{k_{\mathrm{sp}}}{h}\tanh(\ th_{\mathrm{sp}})}{1 + \frac{k_{\mathrm{sp}}}{h}\tanh(\ th_{\mathrm{sp}})}\right] \quad [20]$$

where

$$\beta = \frac{3/2}{\sqrt{A_{\mathrm{evap,base}}}} + \frac{1}{\sqrt{A_{\mathrm{chip}}}} \quad [21]$$

4. RESULTS AND DISCUSSION

The variation of the contributions of the nucleate boiling and convective heat transfer coefficients on the total two-phase heat transfer coefficient as a function of quality is shown in Figure 8. Both the variation of the overall flow boiling heat transfer coefficient and the varying contribution of the nucleate and convection coefficients highlight the impact of the scaling of the contributions of each component of the flow boiling heat transfer coefficient shown in Equation 1.

Next, the critical heat flux is plotted with respect to quality. These results are provided for several geometric parameters in Figure 9.

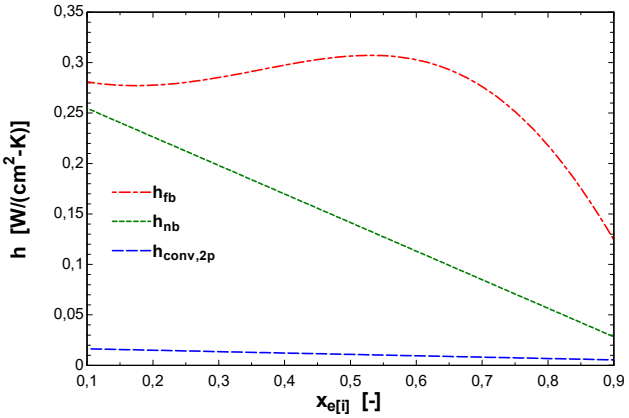

Figure 8: Numerical results of heat transfer coefficient calculations with quality.

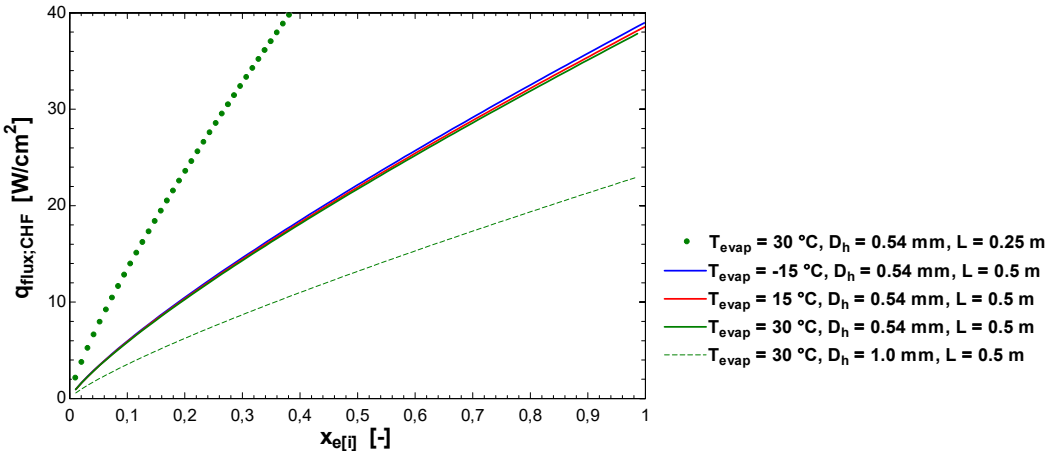

Figure 9: Critical heat flux variations with quality with different geometries and evaporation temperatures.

From Figure 9 it can be seen that the critical heat flux is not significantly affected by the evaporation temperature, but is inversely proportional to the hydraulic diameter and length. This suggests that an intermediate evaporation pressure should be used that is not too low such that the vapor-compression cycle efficiency is compromised but low enough that the convective heat transfer gradient results in a smaller length heat exchanger. The pressure drop is inversely proportional to the hydraulic diameter, therefore multiple rows of larger diameter tubes that are shortened are proposed. This decrease in length not only increases the achievable heat flux but also mitigates the negative heat transfer effects by the larger diameters necessary to decrease pressure drop as much as possible. Furthermore, the evaporator inlet quality should be increased by increasing the pressure differential between the flash tank and the evaporator because this will govern the maximum heat flux that can be solved by this solution. Another balance will need to be reached here, as the increases inlet qualities decrease the overall change in specific enthalpy across the evaporator, thus requiring a higher mass flow rate and compressor input power to absorb the demanded cooling load. The influence of variation in pressure differential between the flash tank and the evaporator is shown in Figure 10, and the corresponding heat flux, assuming 75% of critical heat flux, is shown in Figure 11.

Figure 10 shows that the larger the flash tank pressure differential is the higher the evaporator inlet quality would be. The influence of evaporation pressure on this effect is a function of the slope of the vapor dome at the region of pressures in question, as the flash tank liquid outlet isenthalpically expands to the evaporator inlet from the saturated liquid line of the vapor dome. However, this effect is not so notable that the vapor compression cycle efficiency needs to be compromised for it. Figure 11 further motivates the higher quality evaporator inlet state and corroborates the heat transfer coefficient variation with quality shown in Figure 8. Figure 12 and Figure 13 plot results from the same

parametric study used for Figure 10 and Figure 11, with the flash tank pressure differential direction denoted by accompanying arrows, and show the effects of this variation on the required heat transfer surface area, $A_{evap,base}$, and heat flux with coefficient of performance, COP, respectively. COP is defined as the ratio of cooling capacity of the evaporator to system input power. Fan power is not considered in this analysis, therefore the only system input power considered is the compressor input power and the heater input power when applicable.

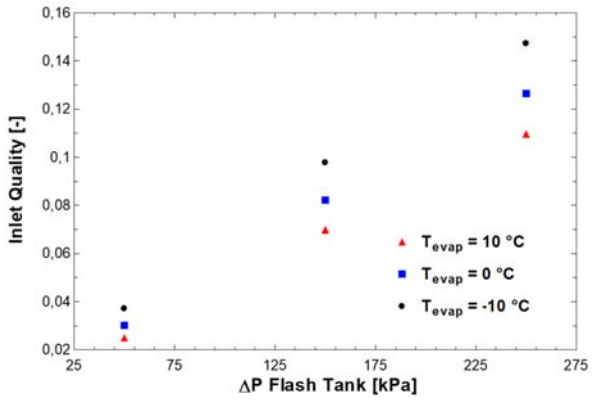

Figure 10: Evaporator inlet quality variation with flash tank and evaporation pressure differential.

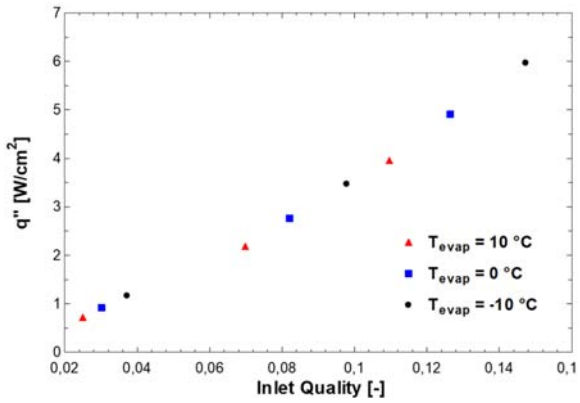

Figure 11: Flow heat flux variation with evaporator inlet quality.

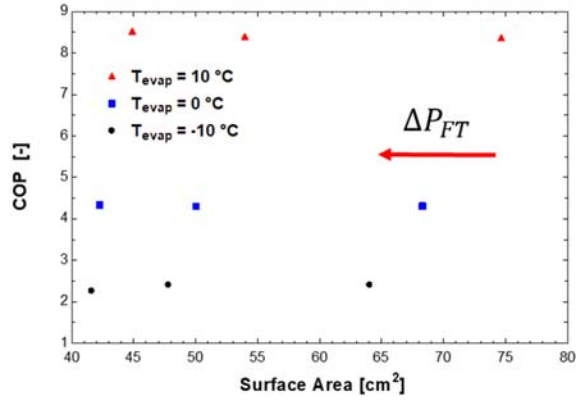

Figure 12: COP and heat transfer surface area relationship with evaporation temperature.

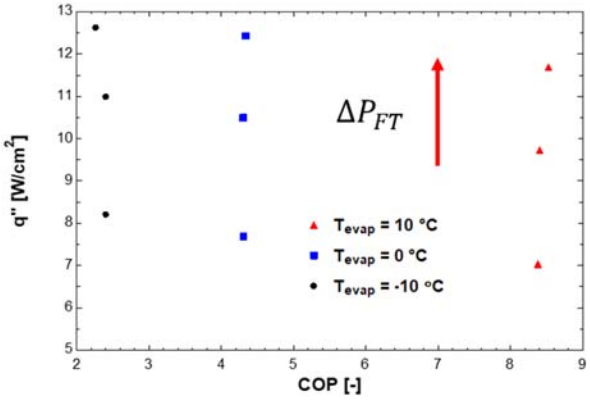

Figure 13: Heat flux and COP relationship with evaporation temperature.

These results confirm that the COP is very sensitive to evaporation pressure. While the lower evaporation pressure has been shown to increase the heat flux absorbed for a given flash tank pressure differential, the improvement was on the order of 10's of percent. Figure 13 shows that the effect of evaporation pressure on COP is on the order of 100's of percent, and that the flash tank pressure differential does not have a significant effect on COP. Therefore, a higher evaporation pressure and a higher pressure differential between the evaporator and flash tank would be the combination that would lead to the highest heat flux and COP. In many cases the evaporation temperature is much closer to the source temperature, but in this application a large temperature difference was desired to maximize the heat transfer gradient between the chip surface temperature of 90 °C and the evaporator temperature. However, if the evaporation temperature were to be set to below 0 °C, then moisture and subsequent freezing effects would need to be taken into consideration. While these relationships are meaningful and conclusive a concrete result from the model was also achieved. A geometry that was conservative but still took advantage of the conclusions listed above was chosen and consists of 8 tubes with a diameter of 2 mm, an evaporation temperature of 5 °C. With a flash tank pressure differential of 250 kPa, this design was able to dissipate 12.55 $\frac{W}{cm^2}$. While this is not a massive value, a spreader that has an area ratio of 10:1 will bring the flux up to 125.5 $\frac{W}{cm^2}$, which is on the same order of magnitude of the target. The target power dissipation of 525 W was reached under all proposed conditions and geometries, as it was treated as a model input.

5. CONCLUSIONS

A microchannel evaporator design tool has been proposed and integrated with a novel vapor-compression cycle to provide both a system and component level detailed solution. The tool can determine the required heat exchanger geometry and length for a given capacity. The interrelations of heat flux and COP with respect to evaporation pressure and heat exchanger geometry were investigated. While increased evaporation temperatures decreased the maximum attainable heat flux, the detrimental impact on heat flux was an order of magnitude smaller than the improvement on COP. Furthermore, decreased characteristic lengths resulted in higher heat fluxes, thus motivating the use of a larger number of short tubes in parallel. A particular concern for this design is that the actual heat exchanger size will be too large for this application. Regardless of heat transfer metrics or attainable heat fluxes, the heat exchanger will be formidable in size and could limit it to applications in super-computing or similar areas where feasible size is not nearly as large of an issue as it is in consumer electronics or even industrial electronics. One remedy to this could be to select a fluid that was still applicable to vapor compression cycles but a more promising heat transfer fluid than R-134a. The design has significant margin in COP due to the small temperature lift across the compressor, so vapor compression performance could be sacrificed in order to increase the applicable heat flux.

The target capacity of 525 W was reached in all conditions and geometries because it was an input for the model. A maximum heat flux reached was 125.5 $\frac{\mathrm{W}}{\mathrm{cm}^2}$ with a heat spreader. While the model is effective, higher evaporator inlet qualities should be implemented to increase the heat flux for the cycle and spreader technologies should be investigated in order to decrease the spreading resistance and increase the effective heat flux. The amount of heat transferred relative to the power required, complemented by the controllability of the evaporator inlet quality, suggests that this vapor compression cycle architecture is promising for future work in this application.

ACKNOWLEDGEMENTS

The authors would like to thank the faculty and staff of Ray W. Herrick Laboratories for technical support.

REFERENCES

Bach, C.K., Groll, E.A., Braun, J.E., Horton, W.T., 2014. Interleaved Circuitry And Hybrid Control As Means To Reduce The Effects Of Flow Maldistribution. Proc. 15th Int. Refrig. Air Cond. Conf.

Bertsch, S.S., Groll, E.A., Garimella, S. V., 2009. A composite heat transfer correlation for saturated flow boiling in small channels. Int. J. Heat Mass Transf. 52, 2110–2118. https://doi.org/10.1016/j.ijheatmasstransfer.2008.10.022

Gwinn, J.P., Webb, R.L., 2003. Performance and testing of thermal interface materials. Microelectronics J. 34, 215–222. https://doi.org/10.1016/S0026-2692(02)00191-X

Joshi, Y., Wei, X., 2005. Micro and meso scale compact heat exchangers in electronics thermal management–a review. Proc. 5th Int. Conf. Enhanc. Compact Ultra Compact Heat Exch. Hoboken, NJ, USA 162–179.

Lee, P.S., Garimella, S. V., 2008. Saturated flow boiling heat transfer and pressure drop in silicon microchannel arrays. Int. J. Heat Mass Transf. 51, 789–806. https://doi.org/10.1016/j.ijheatmasstransfer.2007.04.019

Li, W., Wu, Z., 2010. A general correlation for evaporative heat transfer in micro/mini-channels. Int. J. Heat Mass Transf. 53, 1778–1787. https://doi.org/10.1016/j.ijheatmasstransfer.2010.01.012

Mudawar, I., 2001. Assessment of High-Heat-Flux Thermal 24, 122–141.

Sohel Murshed, S.M., Nieto de Castro, C.A., 2017. A critical review of traditional and emerging techniques and fluids for electronics cooling. Renew. Sustain. Energy Rev. 78, 821–833. https://doi.org/10.1016/j.rser.2017.04.112

Tuo, H., Hrnjak, P., 2012. Flash gas bypass in mobile air conditioning system with R134a. Int. J. Refrig. 35, 1869–1877. https://doi.org/10.1016/j.ijrefrig.2012.05.013

Zhang, H.Y., Mui, Y.C., Tarin, M., 2010. Analysis of thermoelectric cooler performance for high power electronic packages. Appl. Therm. Eng. 30, 561–568. https://doi.org/10.1016/j.applthermaleng.2009.10.020

Zivi, S.M., 1964. Estimation of Steady-State Steam Void-Fraction by Means of the Principle of Minimum Entropy Production. J. heat Transf. 86.

NOMENCLATURE

A	Area	(m^2)	**Acronyms**	
a	Empirical flow boiling constant	$(-)$	COP	Coefficient of Performance
b	Empirical flow boiling constant	$(-)$	EXV	Electronic Expansion Valve
Bl	Boiling number	$(-)$	VCC	Vapor Compression Cycle
C	Martinelli-Chisolm constant	$(-)$	**Subscript**	
Co	Confinement number	$(-)$	2Ø	Two-phase
D	Diameter	(mm)	accel	Acceleration
f_f	Friction factor	$(-)$	CHF	Critical heat flux
G	Mass flux	$\left(\frac{kg}{s-m^2}\right)$	conv	Convective
h	Specific enthalpy, heat transfer coefficient	$\left(\frac{kJ}{kg}\right), \left(\frac{W}{cm^2-K}\right)$	evap	Evaporator
L	Channel length	(m)	e	Equivalent
$\dot{m}$	Mass flow rate	$\left(\frac{kg}{s}\right)$	f	Liquid
n	Number	$(-)$	fb	Flow boiling
p	Pressure	(kPa)	FT	Flash tank
q"	Heat flux	$\left(\frac{W}{cm^2-K}\right)$	g	Vapor
$\dot{Q}$	Heat transfer rate	(W)	h	Hydraulic
R	Thermal resistance	$\left(\frac{K}{W}\right)$	i	Index
T	Temperature	$(°C)$	in	Input
th	Thickness	(m)	NB	Nucleate boiling
tol	Tolerance	(m)	o	Outlet
v	Specific volume	$\left(\frac{m^3}{kg}\right)$	R	Refrigerant
$\dot{W}$	Power	(W)	sp	Spreader
X	Martinelli coefficient	$(-)$	tot	Total
x	Quality	$(-)$	tp	Two-phase
z	Direction	$(-)$	W	Wall
Greek Symbols				
Δ	Change	$(variable)$		
α	Void fraction	$(-)$		
β	Spreading coefficient	$(-)$		
μ	Dynamic viscosity	$\left(\frac{kg}{m-s}\right)$		
ϕ_f^2	Two-phase multiplier	$(-)$		